COMPLEX DYNAMICS AND CIRCUIT IMPLEMENTATION OF AN INFINITE-EQUILIBRIA MEMRISTIVE CHAOTIC SYSTEM

Hai-Yong Cao†, Qing Tu

School of Computer and Information Engineering
Nanchang Institute of Technology
Nanchang 330044, China

Received 21 July 2023, accepted 12 December 2023,
published online 20 December 2023

An infinite-equilibria memristive chaotic system (MCS) with plentiful parameter-relied and initial-relied dynamics is constructed from a six-term three-dimensional (3D) system by leading into a flux-controlled memristor. The stabilities of equilibria and dynamical behaviors are discussed. Period-doubling bifurcation corresponds to system parameters and initial values are investigated to reveal its chaos generation. Infinite coexisting chaotic and periodic attractors are discovered in the system by using bifurcation diagrams and phase portraits. Changing multiple parameters of the system, the oscillation amplitude of variables increase or decrease accordingly, yielding the amplitude control feature. Not only the parameter-relied amplitude control, but also the initial-relied amplitude control is found as well. Moreover, the circuit implementation is given to support the physical existence and reliability of the system.

DOI:10.5506/APhysPolB.54.12-A2

1. Introduction

Memristor which was currently confirmed as the fourth basic component [1] portraying the inherent relationship between magnetic flux and charge has been of latest and significant interest in many disciplinary fields. In the field of chaos research, the memristor was commonly deemed to be the nonlinear resistance with a unique memory function and used to construct chaotic circuits and systems, promoting the chaos research to the new stage of memristive chaotic system (MCS) for gaining desired dynamics, and broadening potential applications. Nowadays, the exploration of MCS has become an important issue with widespread attention. Ioth and Chua [2]

† Corresponding author: `flower00@yeah.net`

first constructed the memristive chaotic oscillator by coupling the memristor, inductor, and capacitor together. Muthuswamy *et al.* [3] substituted the nonlinear resistor in the Chua circuit for a flux-controlled memristor to establish a new chaotic circuit, and proposed the simplest chaotic circuit only with a passive inductor, a passive capacitor, and an active memristor with physical realization [4]. Buscarino *et al.* [5] applied two anti-parallel HP memristors to generate a novel chaotic circuit and discussed its rich dynamics, Minati *et al.* [6] also used a SDC physical memristor to establish a chaotic circuit. Kengne *et al.* [7] constructed a new jerk circuit with a memristive diode bridge and found its symmetric coexisting chaos. To some extent, a memristor can usually simplify the design of chaotic circuits with fewer components and easily yield chaos with different types. In preliminary studies, scholars invested a lot of experience in applying a memristor to upgrade and transform the existing classic chaotic circuits. The general method was to add memristors to the circuits or replace the existing nonlinear elements. With further research, the memristor was regarded as a nonlinear control input introduced into any autonomous chaotic systems and massive MCSs were created. Mezatio *et al.* [8] constructed 6D MCS without equilibrium but with the ability to produce coexisting hidden hyperchaos. Gu *et al.* [9] presented non-equilibrium MCS with a hidden double-wing attractor. Lai *et al.* [10] proposed a new piecewise linear memristor and applied it to yield multi-scroll MCS which can be broken into multiple one-scroll attractors causing extreme multistability. Sun *et al.* [11] constructed an MCS with hypermultistability and used it to design an image encryption algorithm. Some chaotic maps with discrete memristors were conveniently established. Ma *et al.* [12] constructed a hyperchaotic map by embedding a discrete memristor into a 2D square map, which showed that a memristor can strengthen the chaotic feature of the map. Lai *et al.* [13] applied a discrete memristor to the Gaussian map for yielding a new MCS with infinite coexisting hidden hyperchaos, and studied its circuit realization and application in image encryption. The memristor was used as a synapse or electromagnetic radiation to construct a memristive chaotic neural network or chaotic neuron [14, 15]. Previous studies have shown that a memristor can drive the chaotic system to form complex and diverse dynamics, including chaos, hyperchaos, multistability, hidden attractors, multi-scroll attractors, and periodic bifurcation. Thereby, a growing number of scholars have continued to be interested in the study of MCS [16–19].

The study of MCS is an emerging research field with significant scientific value, yet there are many issues that require intensive study. The establishment of new MCS and deep exploration of their dynamics have always been important work remaining strong and extensive interest. Pertinently, this paper is devoted to generate a new MCS with a simple structure and infinite equilibria, which performs abundant parameter-relied and initial-relied dynamics. The infinite coexisting attractors and amplitude-control features are discovered. To the best of our knowledge, the proposed MCS has never been reported before. Compared with some existing chaotic systems, it has a simple structure and is easy to implement by a circuit with fewer components. The discovery of infinite chaotic attractors, parameter-relied and initial-relied offset boosting, parameter-relied and initial-relied amplitude control in the proposed MCS also distinguish it from some existing chaotic systems. The dynamical analysis, circuit implementation, and NIST tests of the system are given. This work will provide some reference for constructing MCS with rich dynamical behaviors, and showing the important influence of memristor on the dynamics of a chaotic system. Section 2 describes the model of MCS. Section 3 and Section 4, respectively give the dynamical analysis, circuit implementation, and NIST tests of MCS. Section 5 summarizes the conclusions of the paper.

2. Model description

Let us consider the VB19 system given in literature [20] whose mathematical model is depicted by the following equations:

$$\begin{cases} \dot{x} = z^2 - ay - byz \,, \\ \dot{y} = cz \,, \\ \dot{z} = x - dz \,, \end{cases} \tag{1}$$

with variables x, y, z and parameters a, b, c, d. It has only one unstable equilibrium and performs chaotic motion with parameters $a = b = c = 1$, $d = 0.8$. Taking system (1) as a prototype and equipping an ideal flux-controlled memristor, a new MCS is established that can be written as

$$\begin{cases} \dot{x} = z^2 - ay - byz \,, \\ \dot{y} = cz \,, \\ \dot{z} = xM(w) - dz \,, \\ \dot{w} = x \,, \end{cases} \tag{2}$$

where w and $M(w)$ are the internal variable and memductance of the memristor. Here, we let $M(w) = p + q|w|$, then the model of memristor can be given as

$$i = M(w)x \,, \qquad \dot{w} = x \,, \tag{3}$$

where i, x, w are respectively considered as the current, voltage, and flux of the memristor. Inspired by such a memristor, system (2) will exhibit more diverse and interesting dynamics than system (1), which will to some extent enhance its potential application values. The structure and dynamics of system (2) and system (1) are different. System (2) is four-dimensional with an additional nonlinear term and infinite equilibria, while system (1) is three-dimensional with only one equilibrium. Although they have similar chaotic attractor shape for some fixed parameter values, their Lyapunov exponents and Lyapunov dimensions are different, which indicate their essential differences. In system (1) exists chaos and parameter-relied offset boosting, while system (2) has more rich dynamical behaviors including infinite coexisting attractors, parameter-relied and initial-relied amplitude control features, parameter-relied and initial-relied offset boosting. Thus, the establishment of system (2) enhances the structural and dynamical complexity of the original system (1). It is an effective example of combining low-dimensional chaotic systems with memristors.

Denote $O(\tilde{x},\tilde{y},\tilde{z},\tilde{w})$ as the equilibrium of system (2), then we can compute that $\tilde{x}=\tilde{y}=\tilde{z}=0$ and $\tilde{w}$ can be any real number. It means that system (2) has infinite equilibria determined by $\tilde{w}$. The Jacobian at O is obtained as

$$E=\begin{pmatrix} 0 & -a & 0 & 0 \\ 0 & 0 & c & 0 \\ M(\tilde{w}) & 0 & -d & 0 \\ 1 & 0 & 0 & 0 \end{pmatrix}$$

and its characteristic equation based on $|\lambda I - E| = 0$ is calculated as

$$\lambda\left[\lambda^3 + d\lambda^2 + cM(\tilde{w})\lambda + acM(\tilde{w})\right] = 0\,. \tag{4}$$

Obviously, $\lambda_1 = 0$ is a root of Eq. (4). If $a > 0$, $b > 0$, $c > 0$, $d > 0$, $M(\tilde{w}) > 0$, and $d > a$, then all the roots of $\lambda^3+d\lambda^2+cM(\tilde{w})\lambda+acM(\tilde{w}) = 0$ have negative real parts. Thus, the O is critically stable according to the Routh–Huwritz criterion otherwise, O is unstable as at least one root of Eq. (4) has a positive real part.

3. Dynamical analysis

This section provides a comprehensive and detailed observation of the parameter-relied and initial-relied dynamical properties of system (2) via some numerical means. The infinite coexisting chaos, period-doubling bifurcation, and amplitude control features of system (2) are revealed. All the simulation results in this section are carried out by the Matlab software platform. The equations of system (2) are solved by the fourth–fifth-order Runge–Kutta method with a fixed step size $\Delta t = 0.01$ and an absolute error bound of 10^{-6} at each step. The simulation time is set to $t \in [0, 1000]$.

3.1. Period-doubling bifurcation

It is universally acknowledged that period-doubling bifurcation is an important path to chaos for autonomous systems. Here, we will visually display the period-doubling bifurcation of system (2) for revealing the process of its chaos generation. Assuming $b = c = d = 1$, $p = 0.8$, $q = -0.1$, and varying $a \in [0.2, 1.2]$, we can plot the bifurcation diagram and Lyapunov exponents (LEs) for the initial value $(1, 1, 1, 1)$ illustrated in Fig. 1, which indicates that system (2) experiences period-doubling bifurcation in pace with the parameter a and finally generates chaos. The phase portraits of periodic-1, periodic-2, periodic-4, and chaotic attractors of system (2), respectively, with $a = 0.2, 0.3, 0.42, 0.5$ shown in Fig. 2 intuitively verify the existence of period-doubling bifurcation as well.

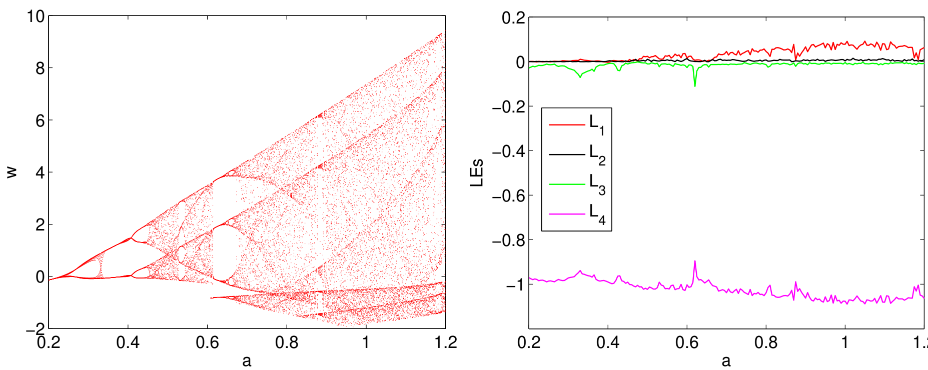

(a) (b)

Fig. 1. Bifurcation diagram and LEs with parameter $a \in [0.2, 1.2]$ for the initial value $(1, 1, 1, 1)$.

System (2) also has initial-relied period-doubling bifurcation. Figure 3 gives the bifurcation diagram and LEs *versus* initial value $(1, 1, 1, m)$ with $m \in [-1, 2]$ under parameter conditions $a = 0.5$, $b = c = d = 1$, $p = 0.8$, $q = -0.1$. Evidently, system (2) enters into a chaotic state via period-doubling bifurcation and traverses the chaotic state via period-doubling bifurcation and then returns to the periodic state with the change of initial value. It can be directly illustrated by plotting the phase portraits with fixed values of $m = -1, -0.5, 0, 0.8, 1.7, 2$, as shown in Fig. 4. It implies that the system's final state is highly dependent on the initial value, thereby system (2) yields coexisting attractors. If the bifurcation diagram continues to change along with m, then infinite coexisting attractors will appear in system (2).

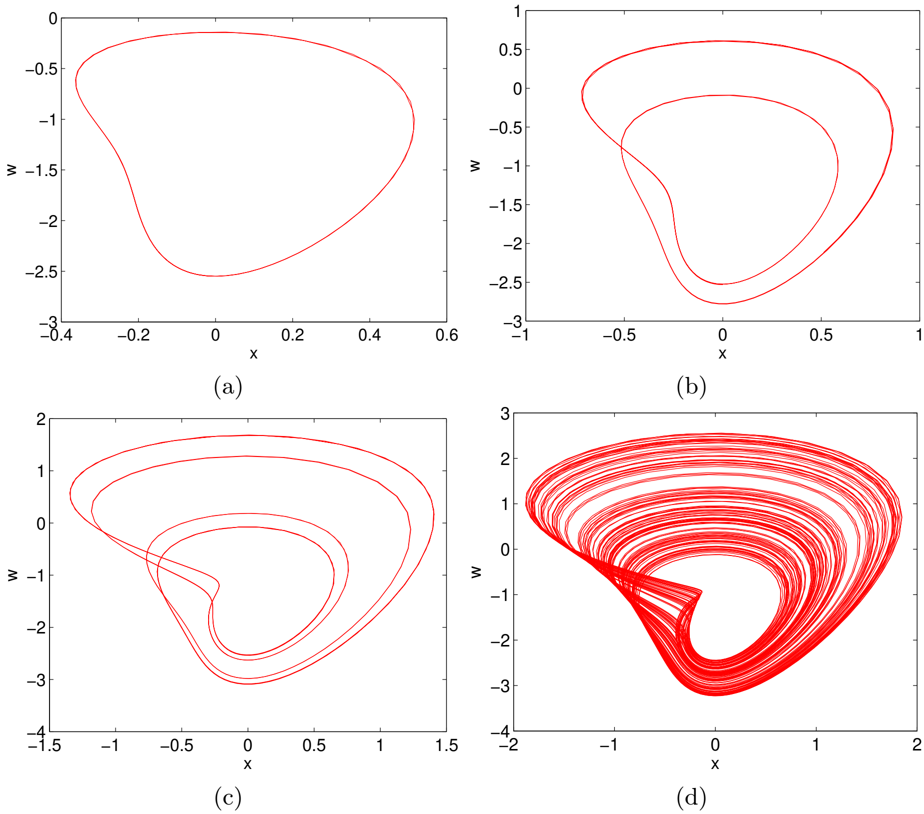

Fig. 2. Phase portraits of system (2) related to period-doubling bifurcation: (a) periodic-1 for $a = 0.20$; (b) periodic-2 for $a = 0.30$; (c) periodic-4 for $a = 0.42$; (d) chaotic for $a = 0.50$.

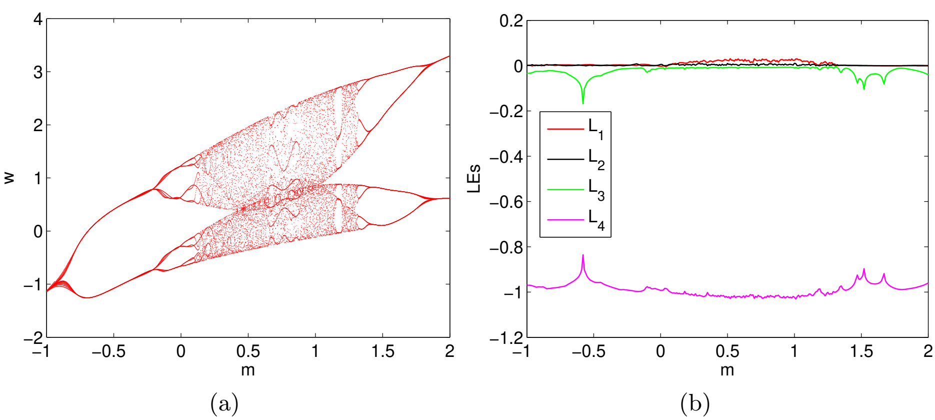

Fig. 3. Bifurcation diagram and LEs *versus* the initial value $(1, 1, 1, m)$ with $m \in [-1, 2]$ for parameters $a = 0.5$, $b = c = d = 1$, $p = 0.8$, $q = -0.1$.

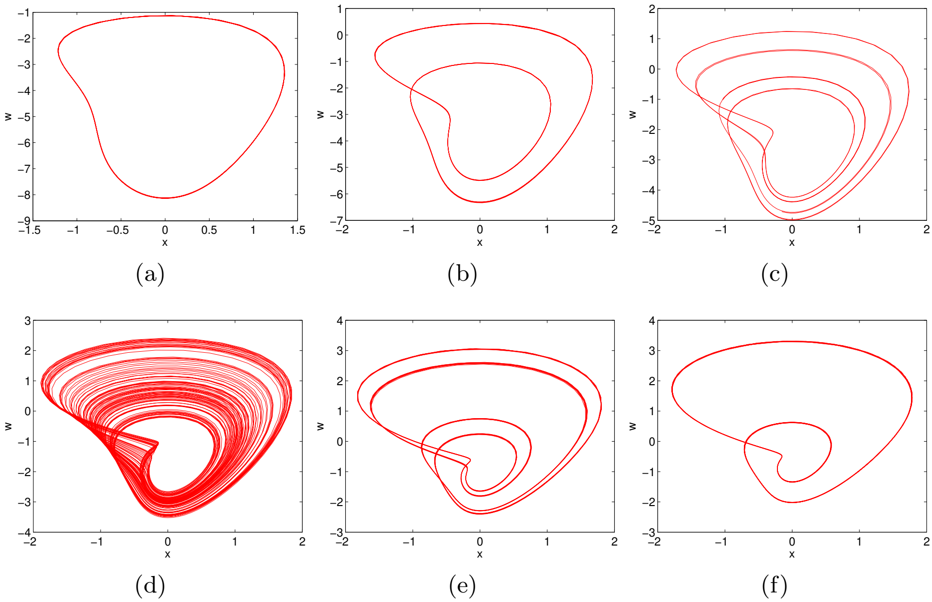

Fig. 4. Phase portraits of system (2) related to period-doubling bifurcation: (a) periodic-1 for $m = -1$; (b) periodic-2 for $m = -0.5$; (c) periodic-4 for $m = 0$; (d) chaotic for $m = 0.8$; (e) periodic-4 for $m = 1.7$; (f) periodic-2 for $m = 2$.

3.2. Infinite coexisting attractors

Fixing the parameters $a = 0.5$, $b = c = d = 1$, $p = 2.5$, $q = -0.1$, and changing the initial value $(1, 1, 1, m)$ with $m \in [-8, 8]$, we can generate the bifurcation diagram of system (2) as shown in Fig. 5 (a), which shows the evolution of final states of system (2) with respect to initial values and verifies the coexistence of infinite chaotic attractors of system (2). Selecting $m = -4, -3, -2, -1, 0$, five attractors with similar shapes and chaotic properties are observed in system (2) which are distributed along the w-axis, as their projections on x–w, z–w and time series of w are shown in Fig. 5 (b)–(d). It can be evidently inferred from Fig. 5 that system (2) has initial-relied offset boosting forming infinite coexisting attractors as the initial value changes with the continuous increase of m. When $a = 0.5$, $b = 1.5$, $c = d = 1$, $p = 2$, and $q = -0.1$, system (2) will generate infinite periodic attractors from initial values with different values of m. Figure 6 (a) shows six periodic attractors in system (2) for $m = -9, -8, -7, -4, -3, -2$. If we reset $b = 1$, then we can observe coexisting two chaotic and two periodic attractors in system (2) for $m = -5, -2, 2, 6$ as given in Fig. 6 (b). Various types of coexisting attractors can emerge in system (2) for other given parameter conditions.

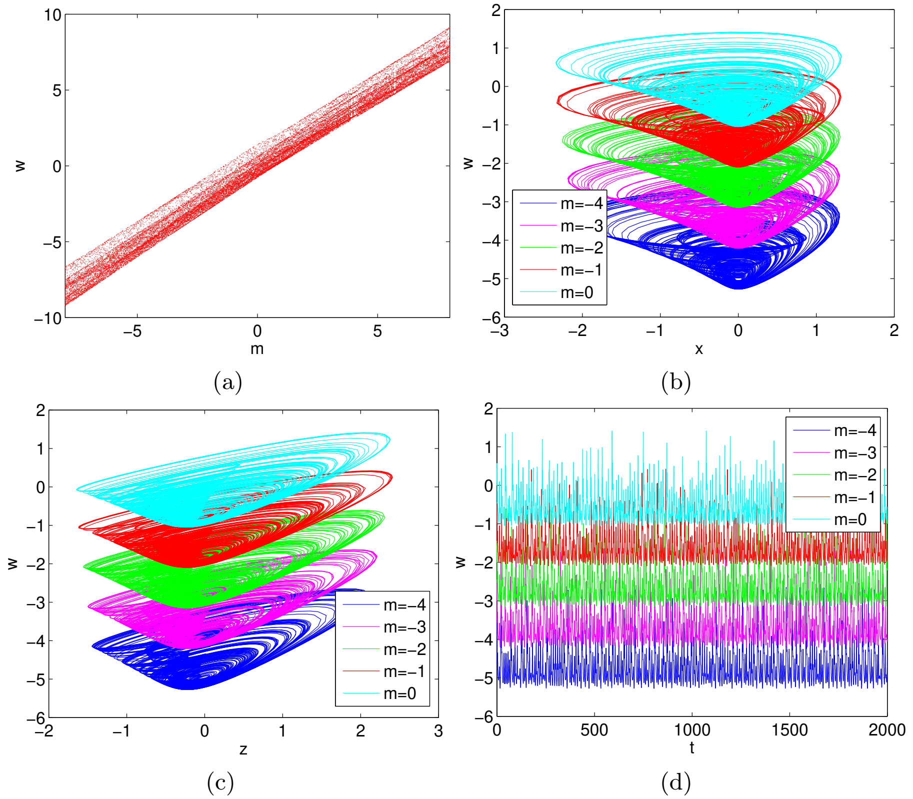

Fig. 5. Coexisting chaotic attractors of system (2) for the initial value $(1, 1, 1, m)$: (a) bifurcation diagram with $m \in [-8, 8]$; (b) projections on x–w for $m = -4, -3, -2, -1, 0$; (c) projections on z–w for $m = -4, -3, -2, -1, 0$; (d) time series of w for $m = -4, -3, -2, -1, 0$.

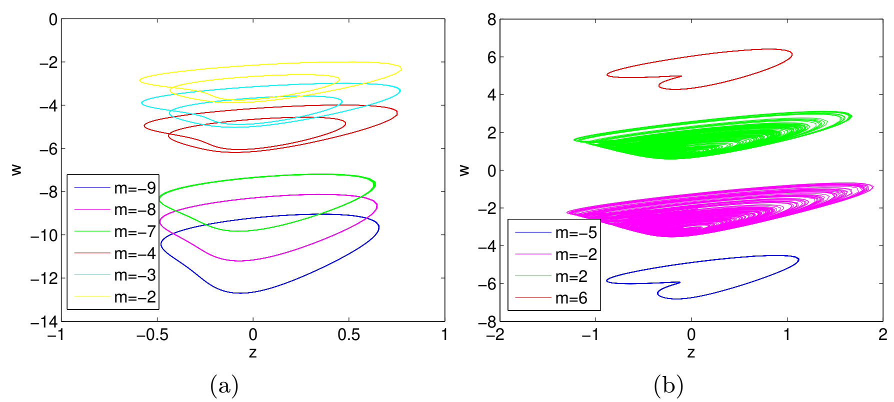

Fig. 6. Coexisting attractors of system (2) for the initial value $(1, 1, 1, m)$: (a) six periodic attractors for $b = 1.5$ and $m = -9, -8, -7, -4, -3, -2$; (b) two chaotic and two periodic attractors for $b = 1$ and $m = -5, -2, 2, -6$.

3.3. Amplitude control features

The parameter-relied and initial-relied amplitude control features of system (2) are studied in this subsection. It shows that the oscillation amplitudes variables of system (2) will increase or decrease with the variations of parameters and initial values when the system is in a chaotic or periodic state. Fixing the initial value (1,1,1,1) and parameters $a = 1$, $c = d = 1$, $p = 2$, $q = -0.1$, we can plot the projections on z–w and time series of w of system (2) with $b = 0.9, 1.0, 1.3, 1.8$, as illustrated in Fig. 7 (a)–(b). Obviously the chaotic signals are shrunk with the increase in b, causing the appearance of amplitude control in system (2). Resetting $a = 0.2$, $p = 0.8$, the amplitude control of periodic signals can be observed by varying $b = 0.5, 0.8, 1.2, 1.8, 2.5$ as shown in Fig. 7 (c)–(d). The amplitude adjustment phenomenon can also be observed by controlling the parameters

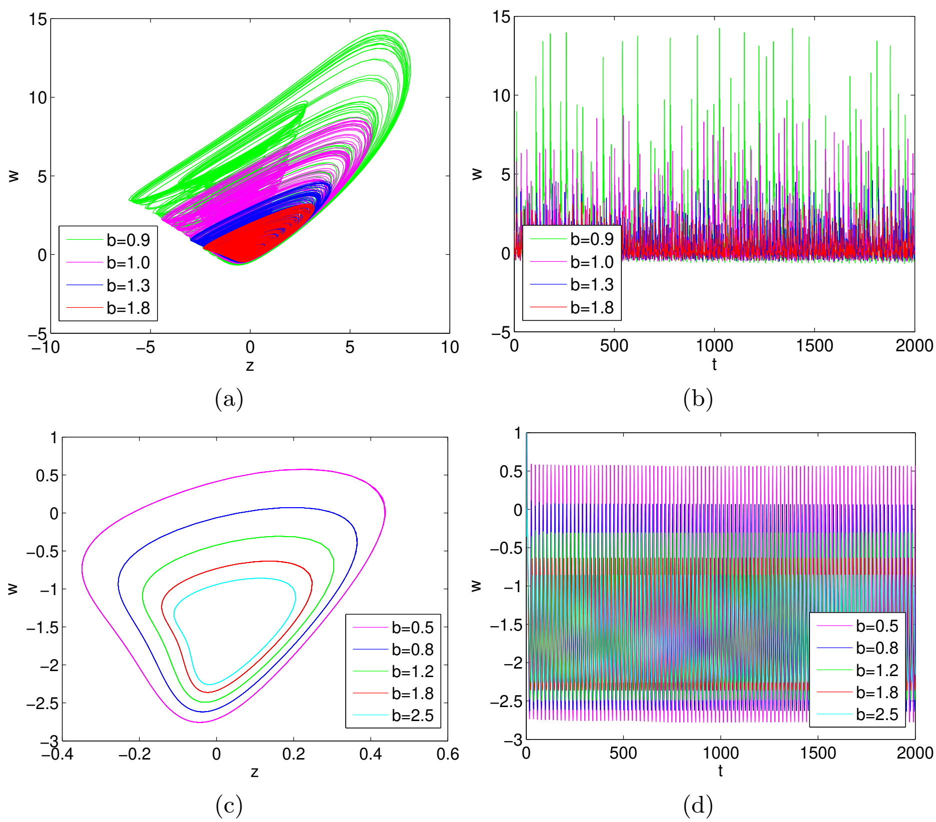

Fig. 7. Amplitude control with the parameter b: (a) and (b) chaotic attractors and time series of w for $b = 0.9, 1.0, 1.3, 1.8$; (c) and (d) periodic attractors and time series of w for $b = 0.5, 0.8, 1.2, 1.8, 2.5$.

c and p. Figure 8 shows the chaotic attractors and time series of y for the parameter values $c = 4.5, 4.0, 3.5, 3.0, 2.0$ and $p = 2.7, 2.6, 2.4, 2.0$, under conditions $a = b = d = 1$, $p = 2$, $q = -0.1$, and initial value $(1, 1, 1, -1)$ and $a = b = c = d = 1$, $q = -0.1$, and initial value $(1, 1, 1, 5)$, respectively. It can be seen that the attractors and time series are decreased with the increase of c or p, which implies the occurrence of parameter-relied amplitude control in system (2). By setting $a = b = c = d = 1$, $p = 2$, $q = -0.1$, we can illustrate the change of attractors and variables for initial values $(1, 1, 1, m)$ with $m = 1, 4, 7, 9$ by using phase portraits and time series, as given in Fig. 9. It is noticeable that the positions of chaotic attractors are shifted in phase space and the oscillation amplitudes of time series decrease while the m increases, which indicates the appearance of initial-relied offset amplitude control in system (2).

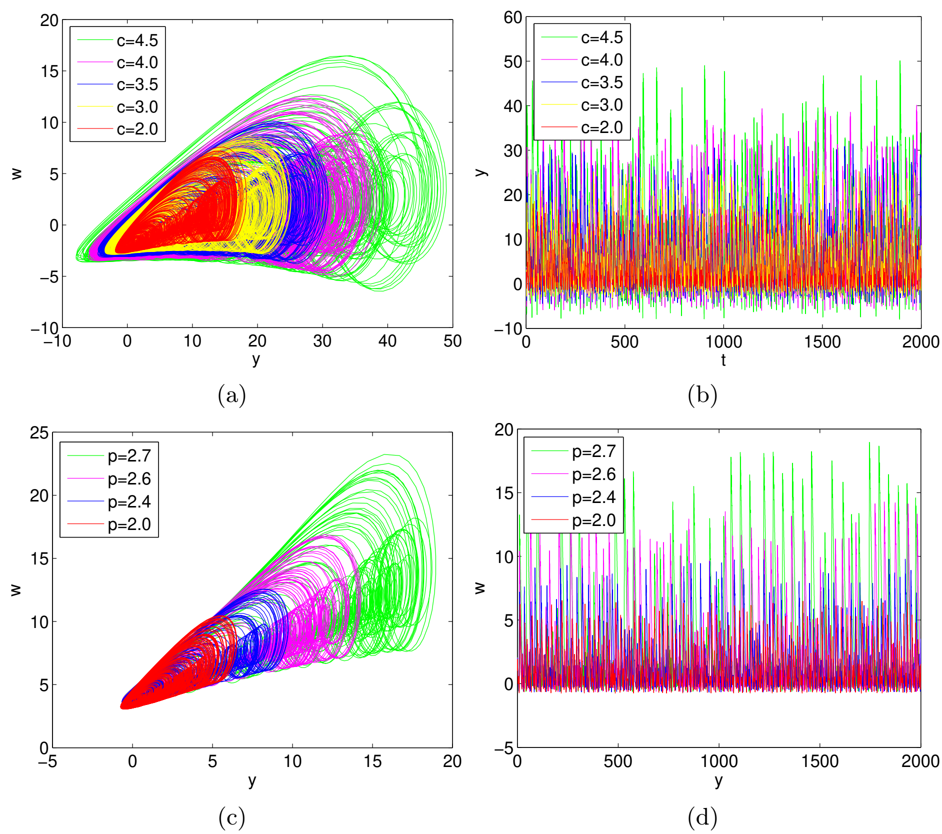

Fig. 8. Amplitude control with the parameters c and p: (a) and (b) chaotic attractors and time series of y for $c = 4.5, 4.0, 3.5, 3.0, 2.0$; (c) and (d) chaotic attractors and time series of y for $p = 2.7, 2.6, 2.4, 2.0$.

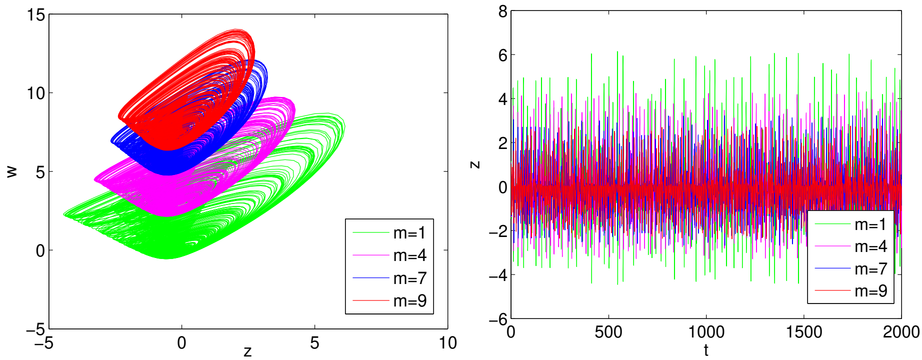

(a) (b)

Fig. 9. Amplitude control for initial values $(1,1,1,m)$ with $m=1,4,7,9$: (a) chaotic attractors; (b) time series of z.

4. Circuit realization and NIST tests

This section presents the circuit realization of system (2) with the help of software and hardware circuit platforms, and studies the National Institute of Standards and Technology (NIST) tests to estimate the randomness of the chaotic sequences. Taking the simulation results shown in Fig. 2 as an example, we will use the electronic circuit to perfectly reproduce these results for physically demonstrating the existence of system (2). The equivalent analog circuit of memristor (3) with an absolute value function is shown in Fig. 10. Based on the basic principles and design methods of circuits, the circuit diagram of system (2) is given in Fig. 11 and its model can be transformed into the following circuit equations:

$$\begin{cases} RC_1\dot{V}_x = -\frac{R}{R_4}\left(-V_z^2\right) - \frac{R}{R_a}V_y - \frac{R}{R_b}V_yV\,, \\ RC_2\dot{V}_y = -\frac{R}{R_c}\left(-V_z\right), \\ RC_3\dot{V}_z = -\left(\frac{R}{R_9}\left(\frac{R(R_q+R)}{R_q(R_p+R)}\right) - \frac{R}{R_q}\left|V_W^2\right|\right)(-V_x) - \frac{R}{R_d}V_z\,, \\ RC_4\dot{V}_w = -\frac{R}{R_f}\left(-V_x\right), \end{cases} \tag{5}$$

where $R = R_4 = R_9 = R_f = 10$ kΩ, $C_1 = C_2 = C_3 = C_4 = 100$ nF and $R/R_a = a$, $R/R_b = b$, $R/R_c = c$, $R/R_d = d$, $R/R_q = q$, $R(R_q + R)/R_q(R_p + R) = p$. When $a = 0.20, 0.30, 0.42, 0.50$, $b = c = d = 1$, $p = 0.8$, $q = -0.1$, then we can calculate $R_a = 50$ kΩ, 33.333 kΩ, 29.809 kΩ, 20 kΩ, $R_b = R_c = R_d = 10$ kΩ, $R_p = 3.75$ kΩ, $R_q = 100$ kΩ, and the same periodic and chaotic attractors given in Fig. 2 can be observed by running the circuit in Fig. 11.

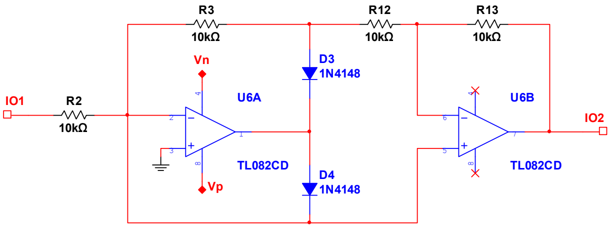

(a)

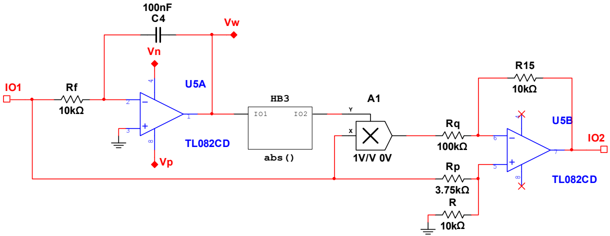

(b)

Fig. 10. Equivalent analog circuits of (a) absolute value function and (b) memristor (3).

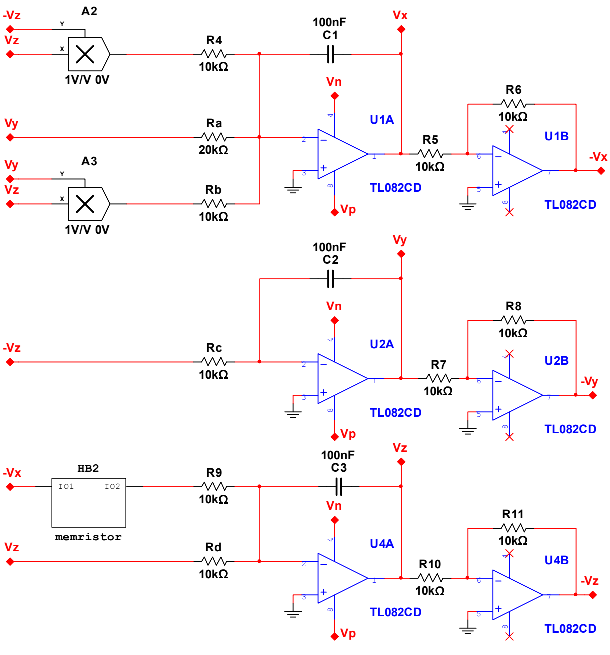

Fig. 11. Circuit diagram of system (2).

Here, the circuit simulation results are based on the Multisim 14 software platform with interactive simulation settings. The initial values of the circuit simulation are automatically set by the software. The step size is fixed as 10^{-5}. The circuit output results are given in Fig. 12 and are highly consistent with the numerical simulation results. Also, we implement system (2) by the microcontroller-based hardware circuit and obtain the corresponding output results as shown in Fig. 13. For other dynamics of system (2) with different parameter conditions, the circuit in Fig. 11 is available as well.

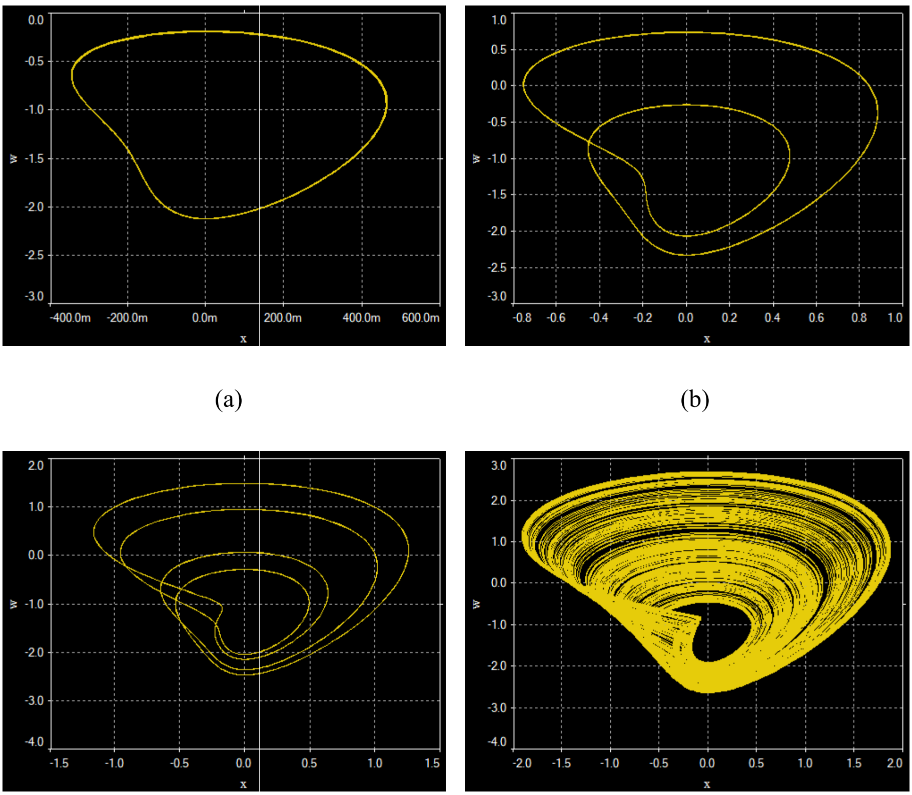

(a) (b)

(c) (d)

Fig. 12. Software circuit output of system (2): (a) periodic-1 for $R_a = 50$ kΩ; (b) periodic-2 for $R_a = 33.333$ kΩ; (c) periodic-4 for $R_a = 23.809$ kΩ; (d) chaotic for $R_a = 20$ kΩ.

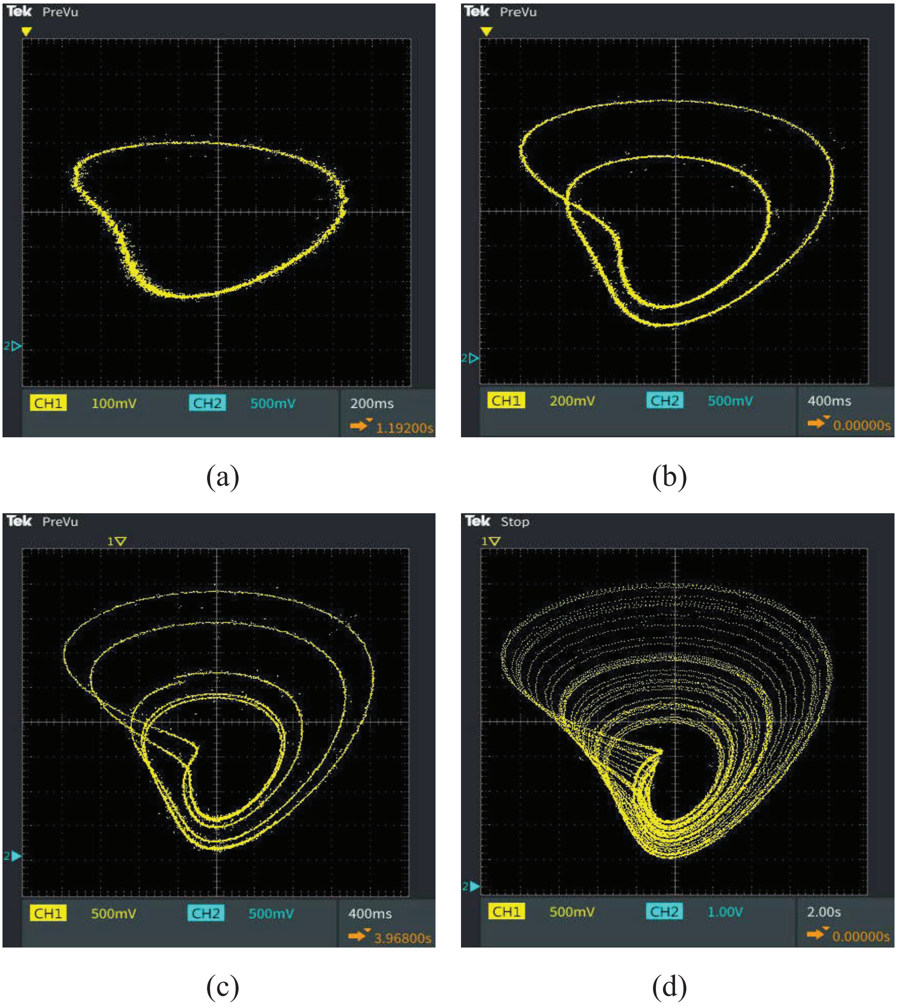

Fig. 13. Hardware circuit output of system (2): (a) periodic-1 for $R_a = 50$ kΩ; (b) periodic-2 for $R_a = 33.333$ kΩ; (c) periodic-4 for $R_a = 23.809$ kΩ; (d) chaotic for $R_a = 20$ kΩ.

Denote the chaotic sequence yielded by system (2) as $X = \{x_1, x_2, \dots x_n\}$, and then convert each of the output x_n to be a 52-bit binary stream XB_n by using the IEEE 754 float standard. Thereby, the digital numbers from 16^{th} to 23^{rd} in a binary stream are taken as the pseudo-random numbers (PRNs) that can be written as $\vartheta_i = XB_{n(16:23)}$. The randomness of the proposed pseudo-random number generator (PRNG) corresponding to system (2) is verified via NIST SP800-22. 120 sets of binary sequences are tested, each with a length of 10^6. The NIST test results are given in Table 1. It is clear that all the pass rates and P-value$_T$ are respectively greater than 0.9628 and 0.0001, which implies that system (2) can generate pseudo-random numbers with a high degree of randomness. To some extent, the feasibility of encryption application of system (2) is demonstrated.

Table 1. NIST test results of the random numbers.

No.	Sub-tests	Pass rate ≥ 0.9628	P-value$_T$ ≥ 0.0001	Result
01	Frequency	0.9917	0.8755	pass
02	Block frequency	0.9917	0.5852	pass
03	Cum. Sum* (F)	0.9917	0.2041	pass
	Cum. Sum* (R)	0.9833	0.5174	pass
04	Runs	0.9833	0.4528	pass
05	Longest runs	0.9917	0.4071	pass
06	Rank	0.9833	0.5174	pass
07	FFT	0.9917	0.9885	pass
08	Non-Ovla. Temp.*	0.9667	0.1005	pass
09	Ovla. Temp.	0.9917	0.1626	pass
10	Universal	0.9917	0.2873	pass
11	Appr. Entropy	0.9833	0.4846	pass
12	Ran. Exc.*	0.9730	0.2475	pass
13	Ran. Exc. Var.*	0.9730	0.0424	pass
14	Serial (1st)	0.9750	0.9411	pass
	Serial (2nd)	0.9917	0.8755	pass
15	Linear complexity	0.9833	0.6718	pass
	Success No.	15/15	15/15	15/15

* Nonoverlapping template test, Random excursions test, and Random excursions variant test contain 148, 8, 18 sub-tests. The worst results are reported for multiple subtests.

5. Conclusions and discussions

This work established a new MCS with infinite unstable equilibria and various interesting dynamics including chaos, period-doubling bifurcation, infinite coexisting attractors, and amplitude control. The dynamical evolution concerning parameters and initial values was investigated by using bifurcation diagrams and phase portraits. It was shown that the proposed MCS can yield period-doubling bifurcation with the variation of parameters or initial values, infinite coexisting chaos in phase space inspired by infinite initial values, and amplitude control which refers to the amplification or reduction of variables by means of changing the parameter values. Moreover, the circuit realization whose output results exactly match the simulation results was given to test the flexibility of the system. So far, the research on MCS has attracted widespread interest and numerous research results of MCS have been obtained. However there are also many issues that need to be further explored. How to design MCS with complex dynamics and how to implement its specific engineering applications are still key tasks that need to be considered and studied. In the future, we will be committed to the construction of new memristor models and used them to design new MCS with different dynamics, such as mutiscroll chaos, hidden chaos, hyperchaos, extreme multistability, amplitude control, *etc.* More theoretical and numerical methods will be used to give a full evaluation of the performance of MCS. The high-security secure communication and encryption technologies based on MCS will be studied. The rich dynamical connotations often determine the application potential of the system, thus it is of great significance to persist in constructing MCS with rich dynamics and delving deeply into its dynamical evolution laws.

REFERENCES

[1] L. Chua, «Memristor — The missing circuit element», *IEEE Trans Circ. Theory* **18**, 507 (1971).

[2] M. Itoh, L.O. Chua, «Memristor Oscillators», *Int. J. Bifurcation Chaos* **18**, 3183 (2008).

[3] B. Muthuswamy, P. Kokate, «Memristor-Based Chaotic Circuits», *IETE Tech. Rev.* **26**, 417 (2009).

[4] B. Muthuswamy, L.O. Chua, «Simplest Chaotic Circuit», *Int. J. Bifurcation Chaos* **20**, 1567 (2010).

[5] A. Buscarino, L. Fortuna, M. Frasca, L.V. Gambuzza, «A chaotic circuit based on Hewlett–Packard memristor», *Chaos* **22**, 023136 (2012).

[6] L. Minati *et al.*, «A chaotic circuit based on a physical memristor», *Chaos Solitons Fractals* **138**, 109990 (2020).

[7] J. Kengne, A. Nguomkam Negou, D. Tchiotsop, «Antimonotonicity, chaos and multiple attractors in a novel autonomous memristor-based jerk circuit», *Nonlinear Dyn.* **88**, 2589 (2017).

[8] B.A. Mezatio *et al.*, «A novel memristive 6D hyperchaotic autonomous system with hidden extreme multistability», *Chaos Solitons Fractals* **120**, 100 (2019).

[9] S. Gu, Q. Peng, X. Leng, B. Du, «A novel non-equilibrium memristor-based system with multi-wing attractors and multiple transient transitions», *Chaos* **31**, 033105 (2021).

[10] Q. Lai, Z. Chen, «Grid-scroll memristive chaotic system with application to image encryption», *Chaos Solitons Fractals* **170**, 113341 (2023).

[11] J. Sun *et al.*, «A Memristive Chaotic System With Hypermultistability and Its Application in Image Encryption», *IEEE Access* **8**, 139289 (2020).

[12] Y. Ma *et al.*, «A Discrete Memristor Coupled Two-dimensional Generalized Square Hyperchaotic Maps», *Fractals* **31**, 2340136 (2023).

[13] Q. Lai, L. Yang, Y. Liu, «Design and realization of discrete memristive hyperchaotic map with application in image encryption», *Chaos Solitons Fractals* **165**, 112781 (2022).

[14] S. Qiao, C. Gao, «Complex dynamics of a non-smooth temperature-sensitive memristive Wilson neuron model», *Commun. Nonlinear Sci. Numer. Simul.* **125**, 107410 (2023).

[15] Q. Lai, Z. Wan, P.D.K. Kuate, «Generating Grid Multi-Scroll Attractors in Memristive Neural Networks», *IEEE Trans. Circ. Syst. I* **70**, 1324 (2023).

[16] B. Liang *et al.*, «A 3D chaotic system with multi-transient behavior and its application in image encryption», *Physica A* **616**, 128624 (2023).

[17] X. Liu, K. Sun, H. Wang, S. He, «A class of novel discrete memristive chaotic map», *Chaos Solitons Fractals* **174**, 113791 (2023).

[18] D.V. Hoang *et al.*, «Building discrete maps with memristor and multiple nonlinear terms», *Integration* **90**, 126 (2023).

[19] K. Cao, Q. Lai, «A Simple memristive chaotic system with complex dynamics and ITS image encryption application», *Int. J. Mod. Phys. B* **36**, 2250131 (2022).

[20] C.B. Li, J.C. Sprott, «Variable-boostable chaotic flows», *Optik* **127**, 10389 (2016).